

---

# Generalizable Implicit Motion Modeling for Video Frame Interpolation

---

Zujin Guo, Wei Li, Chen Change Loy<sup>✉</sup>  
S-Lab, Nanyang Technological University  
{zujin.guo, wei.l, ccloy}@ntu.edu.sg  
<https://gseandat.github.io/projects/GIMMVFI>

## Abstract

Motion modeling is critical in flow-based Video Frame Interpolation (VFI). Existing paradigms either consider linear combinations of bidirectional flows or directly predict bilateral flows for given timestamps without exploring favorable motion priors, thus lacking the capability of effectively modeling spatiotemporal dynamics in real-world videos. To address this limitation, in this study, we introduce Generalizable Implicit Motion Modeling (GIMM), a novel and effective approach to motion modeling for VFI. Specifically, to enable GIMM as an effective motion modeling paradigm, we design a motion encoding pipeline to model spatiotemporal motion latent from bidirectional flows extracted from pre-trained flow estimators, effectively representing input-specific motion priors. Then, we implicitly predict arbitrary-timestep optical flows within two adjacent input frames via an adaptive coordinate-based neural network, with spatiotemporal coordinates and motion latent as inputs. Our GIMM can be smoothly integrated with existing flow-based VFI works without further modifications. We show that GIMM performs better than the current state of the art on the VFI benchmarks.

## 1 Introduction

Video Frame Interpolation (VFI) is a fundamental task in computer vision, which involves generating intermediate frames between two adjacent video frames. This technique is crucial for various practical applications, including novel view synthesis [53, 14, 29], video generation [44], and video compression [49]. This task is highly challenging due to the complex motions typically found in real-world videos. To address this, recent research [28, 52, 40, 38, 19] has focused on flow-based frameworks, which have shown substantial success. Generally, these frameworks for VFI involve two main phases: 1) transforming the input frames based on estimated optical flows, and 2) merging and enhancing the warped frames to produce intermediate frames. Consequently, the accuracy of flow estimation is crucial for the fidelity of the synthesized frames.

Accurately modeling flow from two distant frames is challenging due to the complexities of capturing subtle and dynamic movements caused by varying motion speeds, object occlusions, and lighting conditions. A commonly used approach in the literature combines bidirectional flows derived from input frames [21, 38, 42, 50, 37] (Figure 1(a)). This method assumes *overlapped* and linear motion for flow estimation, which does not accurately reflect real-world dynamics. Several studies [19, 28, 52, 40] directly predict bilateral flows based on intermediate discrete timestamps (Figure 1(b)). These approaches model the correlation between frame motions and timestamps without leveraging motion priors within input frames; they thus fall short in capturing complex spatial-temporal changes and handling occluded regions and unexpected deformations. Moreover, this discrete-time-based modeling paradigm is ineffective for arbitrary-time interpolation.

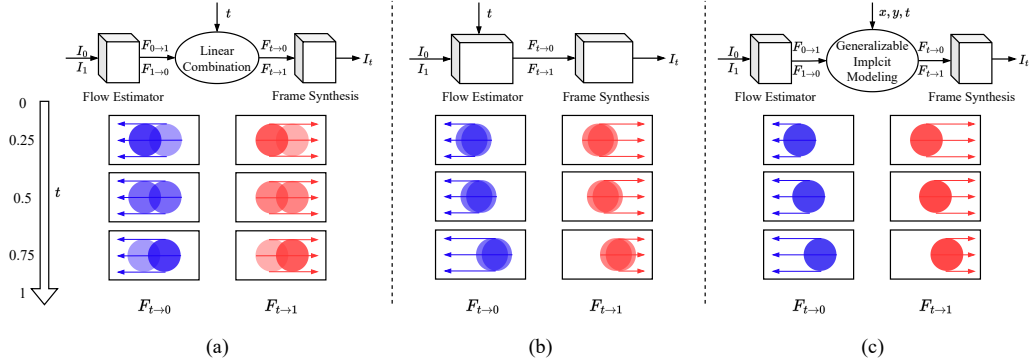


Figure 1: **Schematic of motion modeling paradigms** in video frame interpolation. **(a)** A naïvely *linear combination* of bidirectional flows  $F_{0 \rightarrow 1}, F_{1 \rightarrow 0}$  (i.e., flows between input frames) may lead to ambiguous and coarse motion estimation, due to strong overlapped and linear assumptions. **(b)** A *time-condition-based modeling* approach may predict suboptimal bilateral flows  $F_{t \rightarrow 0}, F_{t \rightarrow 1}$  (i.e., flows between estimated and input frames), capturing spatiotemporal changes for moving objects ineffectively. **(c)** Our *generalizable implicit motion modeling* can properly represent spatiotemporal dynamics across videos and predict better bilateral flows via an adaptive coordinate-based neural network.

In this study, we explore a more effective and generalizable approach to motion modeling for VFI. Inspired by the success of implicit neural representations [45] in encoding complex high-dimensional data such as 2D images [5], 3D scenes [32], and videos [3], we propose to implicitly model optical flows between two adjacent video frames using coordinate-based neural networks. This implicit paradigm can directly take arbitrary spatiotemporal coordinates as inputs and effectively decode the desired space-time outputs, making it a promising framework for learning highly dynamic optical flows in real-world videos. However, leveraging implicit neural networks for effective motion modeling poses challenges. First, standard implicit neural networks typically perform per-instance modeling, optimizing model parameters for a single specific input. This limitation restricts their applicability across different input video frames. Therefore, we need to develop a more adaptive implicit model capable of capturing motions in any given video. Second, efficiently integrating spatiotemporal information within implicit neural networks is complex, especially when dealing with the intricate motions occurring between two video frames. This necessitates designing appropriate implicit neural architectures that can accurately predict and represent both the spatial and temporal dynamics in videos.

To this end, we propose a novel generalizable implicit flow encoding for motion modeling in VFI, called Generalizable Implicit Motion Modeling (GIMM) (Figure 1(c)). Our method only assumes the availability of bidirectional flows ( $F_{0 \rightarrow 1}, F_{1 \rightarrow 0}$ ) of two input frames obtained from a pre-trained optical flow estimator (e.g., RAFT [47], FlowFormer [18]). The input flows can be noisy as this prior will be refined to estimate the bilateral flows ( $F_{t \rightarrow 0}, F_{t \rightarrow 1}$ ) between arbitrary intermediate timestamps. Our method is unique in that it can represent input-specific motion priors effectively, for instance, it can accurately capture the complex dynamics of a somersault. This is achieved by introducing a motion encoding pipeline to extract spatiotemporal motion latents from the bidirectional flows. Our method can further enable frame interpolation at arbitrary timestamps, thanks to the adaptive coordinate-based neural network that takes spatiotemporal coordinates and motion latents as inputs. This capability allows our method to generate frames at various temporal granularities, providing flexibility and precision in video frame interpolation.

Our contributions are summarized as follows: We present an effective motion modeling paradigm for video frame interpolation, characterized by a novel generalizable implicit motion modeling framework (GIMM). Our GIMM is capable of accurately predicting optical flow for arbitrary timesteps between two adjacent video frames at any resolution, allowing seamless integration with existing flow-based VFI methods. We demonstrate the advantages of our GIMM in motion modeling for arbitrary-timestep VFI tasks, achieving state-of-the-art performances on various benchmarks.

## 2 Related Work

**Video frame interpolation.** Conventional VFI studies primarily rely on either direct frame synthesis via convolutional networks [11, 1, 23] or interpolation using dynamic kernels with learnable weights and offsets [35, 36, 39, 9, 8, 12, 27]. Recent approaches have shifted towards flow-based methods to synthesize frames at desired timesteps, where motion modeling plays a crucial role [19, 28, 51, 25, 46, 16]. Some flow-based methods combine estimated bidirectional flows between input frames [21, 38, 42, 50, 37, 1], often leading to inaccurate motion predictions, especially in occluded areas. This simplistic combination results in ambiguous and coarse motion estimation, causing object shifts in interpolated frames. Several recent approaches [19, 28, 52, 19, 30] address these issues by directly predicting the desired motion within an end-to-end framework conditioned on timesteps, showing impressive results in synthesized frames. However, these methods mainly rely on discrete-time-based fitting of variable relationships between motion and timesteps, making it challenging to achieve consistent, continuous interpolation outcomes.

**Implicit neural representations.** Implicit Neural Representations (INRs) have been shown effective in modeling complex, high-dimensional data for various applications, including video compression [3], novel view synthesis [32, 29], and image super-resolution [5]. Typically, INRs learn a continuous mapping from a set of coordinates to a specific signal using a coordinate-based neural network to implicitly encode data. The flexible and expressive modeling capabilities of INRs motivate us to explore their use to encode intricate motions and capture subtle, dynamic movements of objects in real-world videos. A recent work related to ours is IFE [13]. While both approaches consider implicit flow encoding, our method significantly differs from IFE. Unlike IFE, which focuses on per-scene encoding—where each coordinate-based network is parameterized by a specific video instance—we aim to develop a generalizable motion modeling approach that can be applied across different videos.

**Generalizable INRs.** Recent works [5, 41, 10, 20, 15, 7, 4] further extend INRs for generalizable encoding by conditioning coordinate-based neural networks with additional instance-specific inputs. For example, some approaches [6, 26, 24] employ Transformers [48] as meta-learners to predict instance-specific weights or modulation features for coordinate-based neural networks at high computational costs. Several notable studies [4, 7, 42] leverage generalizable INRs for video encoding to facilitate video interpolation and super-resolution, mainly focusing on directly learning implicit space-time continuous neural representations from video. In contrast, we aim to explore effective motion modeling paradigms to improve intermediate frame synthesis for flow-based VFI. To our knowledge, we make the first attempt to utilize generalizable INRs for motion modeling in the context of VFI.

## 3 Method

This section describes our GIMM framework for video frame interpolation. In Sec. 3.1, we first introduce a typical general flow-based VFI process. We subsequently detail our proposed GIMM framework in Sec. 3.2. We finally present the integration of GIMM for flow-based VFI in Sec. 3.3.

### 3.1 Preliminary

**Video frame interpolation.** Given a pair of adjacent video frames  $I_0, I_1 \in \mathbb{R}^{H \times W \times 3}$  with timesteps  $\{0, 1\}$ , a general flow-based video frame interpolation process is defined as follows:

$$F_t = \mathcal{G}(I_0, I_1, t), \quad (1)$$

$$I_t = \mathcal{H}(F_t, I_0, I_1), \forall t \in [0, 1], \quad (2)$$

where  $\mathcal{G}$  denotes a motion modeling (or flow estimation) module, and  $\mathcal{H}$  indicates a frame interpolation process under the guidance of estimated motion  $F_t$  at a timestep of  $t \in [0, 1]$  for input frames  $I_0$  and  $I_1$ . In this work, we mainly focus on studying an effective motion modeling framework  $\mathcal{G}$  for flow-based VFI.

### 3.2 Generalizable Implicit Motion Modeling

The goal of GIMM is to estimate bilateral flows  $F_{t \rightarrow 0}, F_{t \rightarrow 1}$  for any timestep  $t \in [0, 1]$ , deriving from initial bidirectional flows  $F_{0 \rightarrow 1}, F_{1 \rightarrow 0}$ :

$$F_{t \rightarrow 0}, F_{t \rightarrow 1} = \mathcal{G}(F_{0 \rightarrow 1}, F_{1 \rightarrow 0}, t), \forall t \in [0, 1], \quad (3)$$

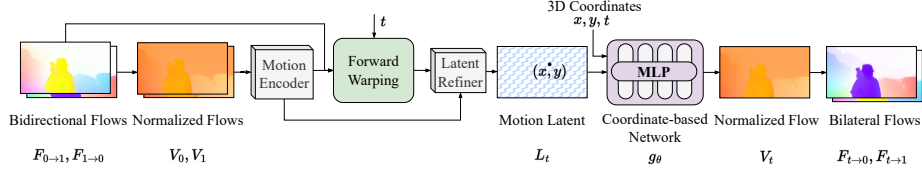


Figure 2: Our GIMM first transforms initial bidirectional flows  $F_{0 \rightarrow 1}, F_{1 \rightarrow 0}$  as normalized flows  $V_0, V_1$ . The motion encoder extracts motion features  $K_0, K_1$  from  $V_0, V_1$ , respectively.  $K_0, K_1$  are then forward warped at a given timestep  $t$  using bidirectional flows to obtain the warped features  $K_{t \rightarrow 0}, K_{t \rightarrow 1}$ . We pass both the warped and initial motion features into a Latent Refiner that outputs motion latent  $L_t$ , representing motion information at  $t$ . Conditioned on  $L_t(x, y)$ , the coordinate-based network  $g_\theta$  predicts the corresponding normalized flow  $V_t$  with 3D coordinates  $\mathbf{x} = (x, y, t)$ . For interpolation usage,  $V_t$  is then transferred into bilateral flows  $F_{t \rightarrow 0}, F_{t \rightarrow 1}$  through denormalization.

where  $F_{0 \rightarrow 1}, F_{1 \rightarrow 0}$  are predicted from a pre-trained optical flow estimator (e.g., RAFT [47], FlowFormer [18]) with input frames  $I_0$  and  $I_1$ . Figure 2 depicts the overall generalizable motion modeling framework of GIMM. Motivated by the great success of INRs in modeling complex video data [7, 4, 13, 32], GIMM uses an adaptive coordinate-based neural network for continuous motion modeling. Unlike the existing IFE [13] that performs per-scene optimization and requires test-time learning for different videos, our GIMM takes additional instance-specific motion latent inputs  $L_t$  to enhance model generalizability across various input videos.

**Flow normalization.** Following IFE [13], we perform normalization for the initial bidirectional flows as follows:

$$V_0 = \phi(F_{0 \rightarrow 1}), V_1 = \phi(-F_{1 \rightarrow 0}), \quad (4)$$

$$V_t = \phi(F_{t \rightarrow 1} - F_{t \rightarrow 0}), \quad (5)$$

where  $\phi$  is a scale operator. This reversible normalization process aligns the scale and temporal direction of input bidirectional flows  $F_{0 \rightarrow 1}, F_{1 \rightarrow 0}$  with output bilateral flows  $F_{t \rightarrow 0}, F_{t \rightarrow 1}$ , allowing the normalized flows  $V_i \in [0, 1]^{H \times W \times 2}, i \in 0, 1$  to be effectively encoded in subsequent implicit motion modeling in GIMM.

**Motion latent.** To achieve generalizable implicit modeling of motion dynamics, we learn implicit neural representations for motions with conditions on instance-specific motion latent inputs  $L_t(x, y)$ , which provides instance-specific motion priors at spatiotemporal coordinates  $\mathbf{x} = (x, y, t)$  for target motion  $V_t(x, y)$ . Specifically, we introduce a Motion Encoder to extract motion features  $K_i$  from normalized flows  $V_i$ . To avoid potential temporal inconsistencies in normalized flows, we derive time-dependent motion features  $K_t$  for given timestep  $t$  from both motion features  $K_0$  and  $K_1$ . To realize this, we apply forward warping  $\vec{w}$  process to map every location of motion features  $K_i$  to the target timestep  $t$ :

$$K_{i \rightarrow t} = \vec{w}(K_i, F_{i \rightarrow t}, Z_i), \quad (6)$$

$$K_{i \rightarrow t}(x, y) = \sum_{a, b} Z_i(a, b) \cdot K_i(a, b), \quad (7)$$

with acquiring warped features  $K_{i \rightarrow t}(x, y)$  at the location  $(x, y)$  includes pairs of spatial coordinates  $(a, b)$  under the constraint of  $F_{i \rightarrow t}(a, b) = (x, y) - (a, b)$ . Here,  $K_{i \rightarrow t}$  are warped features with timesteps  $i \in \{0, 1\}$  that integrate the correspondences from source (input) timesteps to the target timestep,  $Z_i$  represents splatting weights, and  $F_{i \rightarrow t}$  denotes scaled bidirectional flows at timestep  $t$ . We compute scaled bidirectional flows  $F_{i \rightarrow t}$  as follows:

$$F_{i \rightarrow t} = \begin{cases} (t - 0) \cdot F_{0 \rightarrow 1}, & \text{if } i = 0 \\ (1 - t) \cdot F_{1 \rightarrow 0}, & \text{if } i = 1 \end{cases} \quad (8)$$

To mitigate warping errors in multi-to-one cases or occluded regions, we calculate splatting weights  $Z_i$  using flow consistency  $U_{flow}^i$  and variance  $U_{var}^i$  metrics [33, 34] as follows:

$$Z_i = \frac{1}{1 + \alpha_{flow} \cdot U_{flow}^i} + \frac{1}{1 + \alpha_{var} \cdot U_{var}^i}, \quad (9)$$

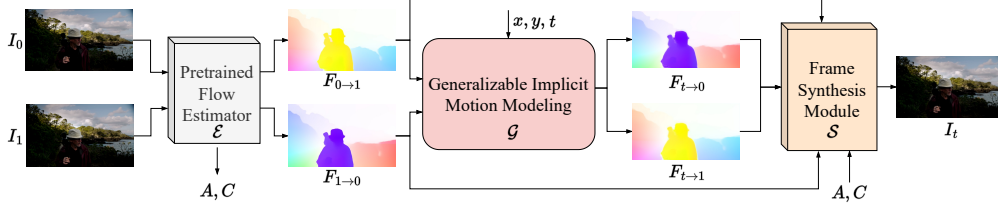


Figure 3: An overview of GIMM-VFI architecture. GIMM-VFI employs a pre-trained flow estimator,  $\mathcal{E}$ , to predict bidirectional flows ( $F_{0 \rightarrow 1}, F_{1 \rightarrow 0}$ ) and extracts context features  $A$  as well as correlation features  $C$  from the input frames ( $I_0, I_1$ ). Given the timestep  $t$ , a generalizable implicit motion modeling (GIMM) module  $\mathcal{G}$  (detailed in Figure 2) takes the bidirectional flows as inputs and predicts bilateral flows ( $F_{t \rightarrow 0}, F_{t \rightarrow 1}$ ), which are then passed into a frame synthesis module  $\mathcal{S}$ , together with extracted features ( $A, C$ ), to synthesize the target frame  $I_t$ .

where  $\alpha_{flow}$  and  $\alpha_{var}$  are learnable parameters. To obtain the final motion latent  $L_t$ , we concatenate the warped features  $\text{Concat}(K_{0 \rightarrow t}, K_{1 \rightarrow t})$  as the coarse motion latent at timestep  $t$  and further refine via a Latent Refiner module to deal with potential information loss and ambiguous motion in the forward warping process. Both the Latent Refiner and the Motion Encoder mentioned above are structured as shallow convolutional networks. We provide their network configurations and detailed calculations for two flow metrics  $U_{flow}^i$  and  $U_{var}^i$  in the supplementary.

**Implicit motion prediction.** To realize INRs for generalizable motion modeling, we devise an adaptive coordinate-based network  $g_\theta$  for implicit and continuous motion encoding, which maps spatiotemporal coordinates  $\mathbf{x} = (x, y, t)$  along with the corresponding motion latent code  $L_t$  to predicted normalized flows  $\hat{V}_t$ :

$$\hat{V}_t = g_\theta(\mathbf{x}, L_t). \quad (10)$$

The predicted normalized flow  $V_t$  can be converted into predicted bilateral flows  $F_{t \rightarrow 0}, F_{t \rightarrow 1}$  via the reverse flow normalization process for VFI. See the supplementary for the details of the coordinate-based network.

**Optimization.** In practice, we optimize the GIMM module by minimizing a Mean-Square-Error (MSE) loss between predicted ( $\hat{V}_t$ ) and ground-truth ( $V_t$ ) normalized optical flows:

$$\mathcal{L}_{gimm}(V_t, \hat{V}_t) = \frac{1}{H \times W} \sum_{k=0}^{H-1} \sum_{l=0}^{W-1} \|V_t(k, l) - \hat{V}_t(k, l)\|_2. \quad (11)$$

### 3.3 Integrating GIMM with Frame Interpolation

**GIMM-VFI.** Given two adjacent video frames  $I_i$  with  $i \in \{0, 1\}$ , we start with a pre-trained optical flow estimator (e.g., RAFT [47], FlowFormer [18]) to extract context features  $A_i$ , correlation features  $C_i$ , and initial bidirectional flows  $F_{0 \rightarrow 1}$  and  $F_{1 \rightarrow 0}$ . We first predict bilateral flows  $F_{t \rightarrow i}$  for a given timestep  $t$  from initial bidirectional flows using a pre-trained GIMM module. The predicted bilateral flows  $F_{t \rightarrow i}$ , context features  $A_i$ , and correlation features  $C_i$  are then passed into a frame synthesis module  $\mathcal{S}$  (adapted from the AMT [28]), which refines the input flows and generates warping masks  $M_t \in [0, 1]^{H \times W}$ . Following previous flow-based VFI studies [28, 52, 40, 19], we obtain warped images  $I_{t \rightarrow i}$  via backward warping  $\overleftarrow{w}$  under the guidance of predicted bilateral flows  $F_{t \rightarrow i}$  from input frames  $I_0$  and  $I_1$ :

$$I_{t \rightarrow i} = \overleftarrow{w}(I_i, F_{t \rightarrow i}), \quad (12)$$

$$I_{t \rightarrow i}(x, y) = I_i(x + F_{t \rightarrow i}^h(x, y), y + F_{t \rightarrow i}^v(x, y)), \quad (13)$$

where  $F_{t \rightarrow i}^h, F_{t \rightarrow i}^v$  represents horizontal and vertical motion of  $F_{t \rightarrow i}$ , respectively. To generate the final interpolated image  $\hat{I}_t$ , the warped images  $I_{t \rightarrow 0}, I_{t \rightarrow 1}$  are fused with the warping mask  $M_t$  as follows:

$$\hat{I}_t = M_t \cdot I_{t \rightarrow 0} + (1 - M_t) \cdot I_{t \rightarrow 1}. \quad (14)$$

See the supplementary for the details of the frame synthesis module.

**Overall objectives.** We use the following objective function for VFI:

$$\mathcal{L}_{interp}(I_t, \hat{I}_t) = \mathcal{L}_{lap}(I_t, \hat{I}_t) + \mathcal{L}_{char}(I_t, \hat{I}_t) + \mathcal{L}_{census}(I_t, \hat{I}_t), \quad (15)$$

where  $\mathcal{L}_{lap}$ ,  $\mathcal{L}_{char}$ , and  $\mathcal{L}_{census}$  denote the Laplacian loss [52, 34], Charbonnier loss [28, 2], and census loss [28, 31], respectively. In addition, to preserve the motion modeling in the pre-trained GIMM module, we reconstruct and supervise the flows  $\hat{V}_0, \hat{V}_1$  with pseudo ground truth  $V_0, V_1$ . This objective  $\mathcal{L}_{rec}$  is defined as  $\|V_0 - \hat{V}_0\|_2 + \|V_1 - \hat{V}_1\|_2$ . The overall objective  $\mathcal{L}$  is as follows:

$$\mathcal{L} = \mathcal{L}_{interp}(I_t, \hat{I}_t) + \lambda_{rec}\mathcal{L}_{rec}, \quad (16)$$

where  $\lambda_{rec}$  is the hyperparameter. We optimize the entire GIMM-VFI model that contains the pre-trained flow estimator, pre-trained GIMM module, and frame synthesis module.

## 4 Experiments

We present quantitative and qualitative evaluations of our motion modeling method GIMM in Section 4.1, and the corresponding interpolation method (GIMM-VFI) in Section 4.3. Specifically, we evaluate both motion quality and performance on the downstream interpolation task. We compare GIMM-VFI with current state-of-the-art VFI methods on arbitrary-timestep interpolation.

**Implementation details.** We train the GIMM model on the training split of Vimeo90K [51] triplets dataset using optical flows extracted by off-the-shelf flow estimators. Our GIMM-VFI is trained on the complete Vimeo90K septuplet dataset. Specifically, we implement two variants of GIMM-VFI, using two different flow estimators: the RAFT [47] and FlowFormer [18], designated as GIMM-VFI-R and GIMM-VFI-F, respectively. More details are provided in the supplementary materials.

### 4.1 Motion modeling

**VTF and VSF benchmarks.** To assess the modeled motion quality with GIMM, we use FlowFormer [18] to produce pseudo ground truth motion. Specifically, we establish two motion evaluation benchmarks: Vimeo-Triplet-Flow (VTF) and Vimeo-Septuplet-Flow (VSF). These benchmarks are derived from the triplet and septuplet splits of the Vimeo90K [51] test set, tailored for evaluating 2X and 6X motion modeling, respectively.

**Baselines.** We compare GIMM with other motion modeling approaches, including *Linear*, *Forward Warp*, and *End-to-End*. Specifically, *Linear* replaces our GIMM module with the linear approximation strategy [21]. Similarly, *Forward Warp* substitutes GIMM with a forward warping strategy [33]. Meanwhile, the *End-to-End* denotes the strategy that directly predicts motion at arbitrary timesteps through an end-to-end fitting. In this end-to-end setting, we select the current state-of-the-art EMA-VFI [52] as the representative method. For fair comparisons, we employ RAFT [47] as the flow estimator for different motion modeling methods.

**Evaluation settings.** We measure the modeled motion quality on both VTF and VSF benchmarks, by calculating PSNR on normalized flows and End-Point-Error (EPE) on the unscaled flows. For the downstream interpolation task, we calculate PSNR on the ‘hard’ split of the SNU-FILM-arb benchmark (SNU-FILM-arb-Hard). Details about SNU-FILM-arb are presented in Section 4.3.

**Results.** We provide quantitative comparisons of our GIMM and baselines in Table 1. We first report the results of motion quality on VTF and VSF. We find that GIMM can continuously model motions in videos. GIMM predicts the best flows on both the VTF benchmark (37.56dB PSNR/ 0.34 EPE) and the VSF benchmark (30.45dB PSNR/ 2.68 EPE) that involves unseen timesteps during training. Moreover, our study highlights the importance of motion priors in both motion modeling and the downstream interpolation task. The *Linear*, *Forward Warp*, and our GIMM methods that leverage motion priors from RAFT [47] can provide better motion and interpolation performances than the *End-to-End* across all benchmarks. Notably, GIMM benefits the interpolation task the most and achieves the highest PSNR of 32.62 dB on SNU-FILM-arb-Hard.

**Visualizations.** Besides the quantitative evaluation of motion modeling, we also qualitatively evaluate them on SNU-FILM-arb, as shown in Figure 4. We observe the capacity of GIMM for accurate motion modeling at arbitrary timesteps. Take the Somersault in Figure 4 for example, the ankle flow

Table 1: **Comparisons of different motion modeling methods.** We assess the modeled motion on Vimeo-Triplet-Flow (VTF) and Vimeo-Septuplet-Flow (VSF) by employing PSNR and EPE metrics. Additionally, we demonstrate their impact on the interpolation task by presenting the PSNR values of their interpolation results on the ‘hard’ split of the SNU-FILM-arb dataset.

Motion method	Vimeo-Triplet-Flow (VTF)		Vimeo-Septuplet-Flow (VSF)		SNU-FILM-arb-Hard
	PSNR $\uparrow$	EPE $\downarrow$	PSNR $\uparrow$	EPE $\downarrow$	PSNR $\uparrow$
Linear	35.03	0.44	30.09	2.87	32.42
Forward Warp	32.80	0.47	28.22	3.38	32.31
End-to-End	29.23	1.02	25.99	5.12	32.28
GIMM (-VFI-R)	<b>37.56</b>	<b>0.34</b>	<b>30.45</b>	<b>2.68</b>	<b>32.62</b>

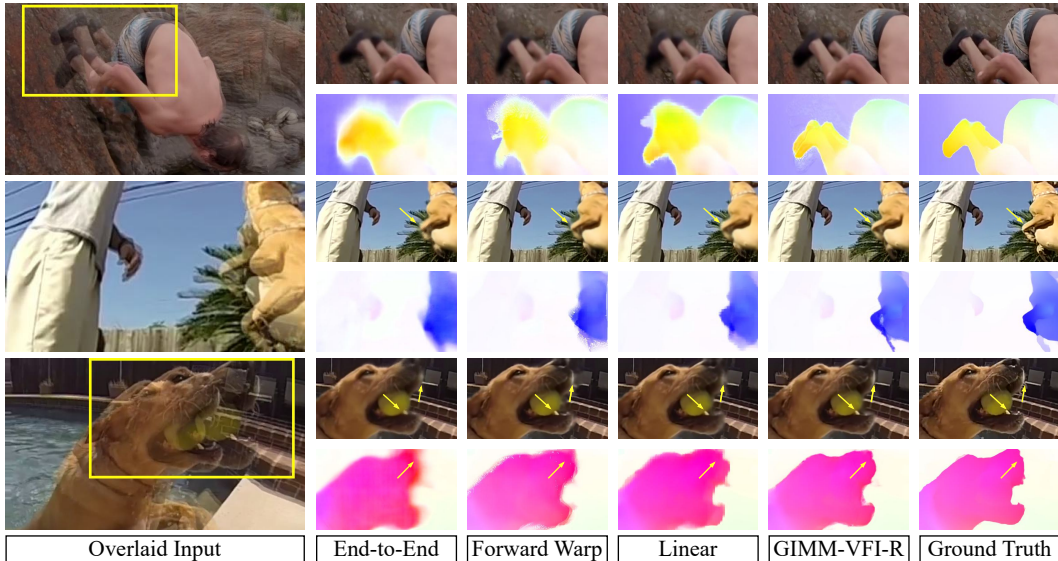


Figure 4: Qualitative comparisons of different motion modeling methods on SNU-FILM-arb-Hard. All the results are predicted at  $t = 0.75$ , and ground truth flows are obtained by FlowFormer [18].

and the corresponding interpolation generated by GIMM have the best consistency with the ground truth, pointing to the same direction. Moreover, GIMM is capable of reducing ambiguities of moving objects. We can observe clearer silhouettes with fewer blurs in both the ‘dog-leg’ and ‘dog-head’ cases in Figure 4.

## 4.2 Ablation Studies

We investigate the effectiveness of model designs in GIMM in Table 2. The experiments are conducted on the Vimeo-Triplet-Flow (VTF) and Vimeo-Septuplet-Flow (VSF).

**Forward warping.** We substitute forward warping operation in GIMM with a straightforward linear combination of the input motion features (*Non-Fwarp*). In Table 2, we observe a significant performance drop with this modification. For example, the EPE on VSF increases by 0.20. This result highlights the importance of forward warping for GIMM’s continuous motion modeling.

**Implicit modeling.** In GIMM, the motion can be modeled even without the presence of implicit modeling. We conduct experiments without using any coordinates (*Non-Imp*). In Table 2, this variant yields performance gains, with reductions of 0.05 and 0.13 in the EPEs on VTF and VSF respectively, highlighting the importance of implicit modeling in GIMM.

**Latent refinement.** To validate the efficacy of latent refinement in GIMM, we conducted experiments excluding the latent refiner (*Non-Refiner*). This led to notable declines of 0.53 dB and 0.43 dB in PSNRs across both benchmarks. Thus, refining the motion latent proves essential for accurate motion modeling.

Table 2: **Quantitative comparisons of different model variants.** For each model variant, we evaluate its motion modeling performance on Vimeo-Triplet-Flow and Vimeo-Septuplet-Flow, respectively. We adopt EPE and PSNR as the metrics for motion quality.

Model Variants	Vimeo-Triplet-Flow (VTF)		Vimeo-Septuplet-Flow (VSF)	
	PSNR $\uparrow$	EPE $\downarrow$	PSNR $\uparrow$	EPE $\downarrow$
Non-Fwarp	37.07	0.37	30.09	2.88
Non-Imp	37.04	0.39	30.11	2.81
Non-Refiner	37.03	0.37	30.02	2.77
T-coord only	37.40	0.36	30.39	2.74
Full	<b>37.56</b>	<b>0.34</b>	<b>30.45</b>	<b>2.68</b>

Table 3: **Quantitative results for arbitrary-timestep interpolation.** We represent the best results in **boldface** and the second best with an underline. The analysis categorizes methods into two groups: non-INR methods (first half) and INR-based methods (second half). We employ a ‘-’ symbol to denote ‘out-of-memory’ scenarios, and a dagger (‘†’) to indicate that the results are drawn from prior studies [19, 17, 52].

Method	XTest		SNU-FILM-arb		
	2K	4K	Medium (4X)	Hard (8X)	Extreme (16X)
RIFE [19]	31.43†	30.58†	36.33	31.87	27.21
IFRNet [25]	31.53†	30.46†	34.88	31.15	26.32
M2M [17]	32.13†	30.88†	36.56	31.92	27.14
AMT [28]	28.88	28.17	34.49	31.03	26.44
UPR-Net [22]	31.16	30.50	36.78	31.96	27.14
EMA-VFI [52]	32.53	31.21	36.65	32.28	27.72
CURE [42]	30.24	-	36.09	31.32	26.61
GIMM-VFI-R	<u>32.71</u>	<u>31.88</u>	<u>37.02</u>	<b>32.62</b>	<u>27.99</u>
GIMM-VFI-F	<b>32.91</b>	<b>31.97</b>	<b>37.03</b>	<u>32.56</u>	<b>28.01</b>

**Spatial coordinates.** We use 3D spatiotemporal coordinates in the implicit modeling of GIMM. To assess the necessity of spatial coordinates, we replace 3D coordinates with temporal coordinates (*T-coord only*). This removal causes a 0.16 dB drop of PSNR on Vimeo-Triplet-Flow and a 0.06 increase of EPE on Vimeo-Septuplet-Flow. This emphasizes the crucial role of spatial coordinates in implicit modeling.

### 4.3 Arbitrary-timestep Video Frame Interpolation

**SNU-FILM-arb benchmark.** We introduce the SNU-FILM-arb benchmark for a more generalized evaluation, to facilitate research on the arbitrary-timestep frame interpolation task. Specifically, we incorporate the SNU-FILM dataset [11] that encompasses 310 clips from 31 videos captured at 240 fps, with heights ranging from 384 to 1280 pixels and widths from 368 to 720 pixels. Different from its original setting of 2X interpolation, we conduct 4X, 8X, and 16X interpolation evaluations on the original ‘Medium’, ‘Hard’, and ‘Extreme’ subsets of SNU-FILM, respectively.

**Evaluation settings.** We calculate PSNR on both SNU-FILM-arb and X4K-1000FPS (XTest) [43]. XTest comprises 15 clips from 15 videos for 8X interpolation. Following the established protocol from prior studies [17, 52], we assess interpolation quality at both 2K and 4K resolutions. For fair comparisons, we disable test-time augmentations during evaluations.

**Current advanced VFI methods.** We compare GIMM-VFI with various advanced interpolation methods. For non-INR methods, we include RIFE [19], IFRNet [25], M2M [17], AMT [28], UPR-Net [22], and EMA-VFI [52]. We also make comparisons with the INR-based method CURE [42].

**Results.** We present the quantitative results of GIMM-VFI on arbitrary-timestep interpolation benchmarks in Table 3. Our proposed method achieves high-quality continuous interpolation across various timesteps (i.e., 4X, 8X, 16X). We observe that our RAFT-based [47] method GIMM-VFI-R achieves significant improvements of **0.18** dB on XTest-2K, **0.67** dB on XTest-4K, and approximately



## References

- [1] Wenbo Bao, Wei-Sheng Lai, Chao Ma, Xiaoyun Zhang, Zhiyong Gao, and Ming-Hsuan Yang. Depth-aware video frame interpolation. In *CVPR*, 2019.
- [2] Pierre Charbonnier, Laure Blanc-Feraud, Gilles Aubert, and Michel Barlaud. Two deterministic half-quadratic regularization algorithms for computed imaging. In *ICIP*, 1994.
- [3] Hao Chen, Bo He, Hanyu Wang, Yixuan Ren, Ser Nam Lim, and Abhinav Shrivastava. NeRV: Neural representations for videos. In *NeurIPS*, 2021.
- [4] Yi-Hsin Chen, Si-Cun Chen, Yen-Yu Lin, and Wen-Hsiao Peng. MoTIF: Learning motion trajectories with local implicit neural functions for continuous space-time video super-resolution. In *ICCV*, 2023.
- [5] Yinbo Chen, Sifei Liu, and Xiaolong Wang. Learning continuous image representation with local implicit image function. In *CVPR*, 2021.
- [6] Yinbo Chen and Xiaolong Wang. Transformers as meta-learners for implicit neural representations. In *ECCV*, 2022.
- [7] Zeyuan Chen, Yinbo Chen, Jingwen Liu, Xingqian Xu, Vidit Goel, Zhangyang Wang, Humphrey Shi, and Xiaolong Wang. VideoINR: Learning video implicit neural representation for continuous space-time super-resolution. In *CVPR*, 2022.
- [8] Xianhang Cheng and Zhenzhong Chen. Video frame interpolation via deformable separable convolution. In *AAAI*, 2020.
- [9] Xianhang Cheng and Zhenzhong Chen. Multiple video frame interpolation via enhanced deformable separable convolution. *IEEE TPAMI*, 2021.
- [10] Julian Chibane, Thiemo Alldieck, and Gerard Pons-Moll. Implicit functions in feature space for 3d shape reconstruction and completion. In *CVPR*, 2020.
- [11] Myungsub Choi, Heewon Kim, Bohyung Han, Ning Xu, and Kyoung Mu Lee. Channel attention is all you need for video frame interpolation. In *AAAI*, 2020.
- [12] Tianyu Ding, Luming Liang, Zhihui Zhu, and Ilya Zharkov. CDFI: Compression-driven network design for frame interpolation. In *CVPR*, 2021.
- [13] Pedro Figueirêdo, Avinash Paliwal, and Nima Khademi Kalantari. Frame interpolation for dynamic scenes with implicit flow encoding. In *WACV*, 2023.
- [14] John Flynn, Ivan Neulander, James Philbin, and Noah Snavely. DeepStereo: Learning to predict new views from the world’s imagery. In *CVPR*, 2016.
- [15] Kyle Genova, Forrester Cole, Avneesh Sud, Aaron Sarna, and Thomas Funkhouser. Local deep implicit functions for 3d shape. In *CVPR*, 2020.
- [16] Xinyu Hou, Liming Jiang, Rui Shao, and Chen Change Loy. Video infilling with rich motion prior. In *BMVC*, 2023.
- [17] Ping Hu, Simon Niklaus, Stan Sclaroff, and Kate Saenko. Many-to-many splatting for efficient video frame interpolation. In *CVPR*, 2022.
- [18] Zhaoyang Huang, Xiaoyu Shi, Chao Zhang, Qiang Wang, Ka Chun Cheung, Hongwei Qin, Jifeng Dai, and Hongsheng Li. FlowFormer: A transformer architecture for optical flow. In *ECCV*, 2022.
- [19] Zhewei Huang, Tianyuan Zhang, Wen Heng, Boxin Shi, and Shuchang Zhou. Real-time intermediate flow estimation for video frame interpolation. In *ECCV*, 2022.
- [20] Chiyu Jiang, Avneesh Sud, Ameesh Makadia, Jingwei Huang, Matthias Nießner, and Thomas Funkhouser. Local implicit grid representations for 3d scenes. In *CVPR*, 2020.

- [21] Huaizu Jiang, Deqing Sun, Varun Jampani, Ming-Hsuan Yang, Erik Learned-Miller, and Jan Kautz. Super SloMo: High quality estimation of multiple intermediate frames for video interpolation. In *CVPR*, 2018.
- [22] Xin Jin, Longhai Wu, Jie Chen, Youxin Chen, Jayoon Koo, and Cheul-Hee Hahm. A unified pyramid recurrent network for video frame interpolation. In *CVPR*, 2023.
- [23] Tarun Kalluri, Deepak Pathak, Manmohan Chandraker, and Du Tran. FLAVR: Flow-agnostic video representations for fast frame interpolation. In *WACV*, 2023.
- [24] Chiheon Kim, Doyup Lee, Saehoon Kim, Minsu Cho, and Wook-Shin Han. Generalizable implicit neural representations via instance pattern composers. In *CVPR*, 2023.
- [25] Lingtong Kong, Boyuan Jiang, Donghao Luo, Wenqing Chu, Xiaoming Huang, Ying Tai, Chengjie Wang, and Jie Yang. IFRNet: Intermediate feature refine network for efficient frame interpolation. In *CVPR*, 2022.
- [26] Doyup Lee, Chiheon Kim, Minsu Cho, and Wook-Shin Han. Locality-aware generalizable implicit neural representation. In *NeurIPS*, 2023.
- [27] Hyeongmin Lee, Taeh Kim, Tae-Young Chung, Daehyun Pak, Yuseok Ban, and Sangyoun Lee. AdaCoF: Adaptive collaboration of flows for video frame interpolation. In *CVPR*, 2020.
- [28] Zhen Li, Zuo-Liang Zhu, Ling-Hao Han, Qibin Hou, Chun-Le Guo, and Ming-Ming Cheng. AMT: All-pairs multi-field transforms for efficient frame interpolation. In *CVPR*, 2023.
- [29] Zhengqi Li, Simon Niklaus, Noah Snavely, and Oliver Wang. Neural scene flow fields for space-time view synthesis of dynamic scenes. In *CVPR*, 2021.
- [30] Liying Lu, Ruizheng Wu, Huaijia Lin, Jiangbo Lu, and Jiaya Jia. Video frame interpolation with transformer. In *CVPR*, 2022.
- [31] Simon Meister, Junhwa Hur, and Stefan Roth. UnFlow: Unsupervised learning of optical flow with a bidirectional census loss. In *AAAI*, 2018.
- [32] Ben Mildenhall, Pratul P. Srinivasan, Matthew Tancik, Jonathan T. Barron, Ravi Ramamoorthi, and Ren Ng. NeRF: Representing scenes as neural radiance fields for view synthesis. In *ECCV*, 2020.
- [33] Simon Niklaus, Ping Hu, and Jiawen Chen. Splatting-based synthesis for video frame interpolation. In *WACV*, 2023.
- [34] Simon Niklaus and Feng Liu. Softmax splatting for video frame interpolation. In *CVPR*, 2020.
- [35] Simon Niklaus, Long Mai, and Feng Liu. Video frame interpolation via adaptive convolution. In *CVPR*, 2017.
- [36] Simon Niklaus, Long Mai, and Feng Liu. Video frame interpolation via adaptive separable convolution. In *ICCV*, 2017.
- [37] Junheum Park, Keunsoo Ko, Chul Lee, and Chang-Su Kim. BMBC: Bilateral motion estimation with bilateral cost volume for video interpolation. In *ECCV*, 2020.
- [38] Junheum Park, Chul Lee, and Chang-Su Kim. Asymmetric bilateral motion estimation for video frame interpolation. In *ICCV*, 2021.
- [39] Tomer Peleg, Pablo Szekely, Doron Sabo, and Omry Sendik. Im-net for high resolution video frame interpolation. In *CVPR*, 2019.
- [40] Fitsum Reda, Janne Kontkanen, Eric Tabellion, Deqing Sun, Caroline Pantofaru, and Brian Curless. FILM: Frame interpolation for large motion. In *ECCV*, 2022.
- [41] Shunsuke Saito, Zeng Huang, Ryota Natsume, Shigeo Morishima, Angjoo Kanazawa, and Hao Li. PIFu: Pixel-aligned implicit function for high-resolution clothed human digitization. In *ICCV*, 2019.

- [42] Wentao Shangquan, Yu Sun, Weijie Gan, and Ulugbek S Kamilov. Learning cross-video neural representations for high-quality frame interpolation. In *ECCV*, 2022.
- [43] Hyeonjun Sim, Jihyong Oh, and Munchurl Kim. XVFI: extreme video frame interpolation. In *ICCV*, 2021.
- [44] Uriel Singer, Adam Polyak, Thomas Hayes, Xi Yin, Jie An, Songyang Zhang, Qiyuan Hu, Harry Yang, Oron Ashual, Oran Gafni, Devi Parikh, Sonal Gupta, and Yaniv Taigman. Make-A-Video: Text-to-video generation without text-video data. *arXiv preprint arXiv:2209.14792*, 2022.
- [45] Vincent Sitzmann, Julien Martel, Alexander Bergman, David Lindell, and Gordon Wetzstein. Implicit neural representations with periodic activation functions. In *NeurIPS*, 2020.
- [46] Li Siyao, Shiyu Zhao, Weijiang Yu, Wenxiu Sun, Dimitris Metaxas, Chen Change Loy, and Ziwei Liu. Deep animation video interpolation in the wild. In *CVPR*, 2021.
- [47] Zachary Teed and Jia Deng. RAFT: Recurrent all-pairs field transforms for optical flow. In *ECCV*, 2020.
- [48] Ashish Vaswani, Noam Shazeer, Niki Parmar, Jakob Uszkoreit, Llion Jones, Aidan N Gomez, Lukasz Kaiser, and Illia Polosukhin. Attention is all you need. In *NeurIPS*, 2017.
- [49] Chao-Yuan Wu, Nayan Singhal, and Philipp Krahenbuhl. Video compression through image interpolation. In *ECCV*, 2018.
- [50] Xiangyu Xu, Li Siyao, Wenxiu Sun, Qian Yin, and Ming-Hsuan Yang. Quadratic video interpolation. In *NeurIPS*, 2019.
- [51] Tianfan Xue, Baian Chen, Jiajun Wu, Donglai Wei, and William T Freeman. Video enhancement with task-oriented flow. *IJCV*, 2019.
- [52] Guozhen Zhang, Yuhan Zhu, Haonan Wang, Youxin Chen, Gangshan Wu, and Limin Wang. Extracting motion and appearance via inter-frame attention for efficient video frame interpolation. In *CVPR*, 2023.
- [53] Tinghui Zhou, Shubham Tulsiani, Weilun Sun, Jitendra Malik, and Alexei A Efros. View synthesis by appearance flow. In *ECCV*, 2016.

## 7 Appendix

In this supplementary material, we first provide details of our method in Section 7.1, including descriptions of flow metrics and reverse flow normalization. Besides, we present the network architectures of both the GIMM module and frame synthesis module in Section 7.2. Moreover, we provide details of our implementation and the corresponding training hyperparameters in Section 7.3 and Section 7.4 respectively. Also, we show qualitative results of motion modeled by GIMM and its model variants in Section 7.5. Finally, we discuss the potential broader impacts in Section 7.6.

### 7.1 Method details

**Flow metrics.** Following Splatting-based Synthesis [33], the implementation of the forward warping operation within our GIMM module leverages flow metrics to enhance its accuracy. More precisely, we employ flow consistency  $U_{flow}^i$ , and flow variance  $U_{var}^i$ . For illustrative purposes, taking  $F_{0 \rightarrow 1}$  as a representative example, we compute its associated metrics as follows:

$$U_{flow}^0 = \|F_{0 \rightarrow 1} + \overleftarrow{\omega}(F_{1 \rightarrow 0}, F_{0 \rightarrow 1})\|_1, \quad (17)$$

$$U_{var}^0 = \|\sqrt{G((F_{0 \rightarrow 1})^2) - G(F_{0 \rightarrow 1})^2}\|, \quad (18)$$

where  $\overleftarrow{\omega}$  is the backward warping operator, and  $G(\cdot)$  denotes a  $3 \times 3$  Gaussian filter.

**Reverse flow normalization.** In GIMM-VFI, we employ reverse flow normalization to convert the predicted normalized flow,  $V_t$ , into bilateral flows for interpolation purposes. This transformation is expressed through the following equations:

$$F_{t \rightarrow 0} = -t \cdot \phi^{-1}(V_t), \quad (19)$$

$$F_{t \rightarrow 1} = (1 - t) \cdot \phi^{-1}(V_t). \quad (20)$$

In this context,  $\phi^{-1}$  represents the scaling operation that extends the value range from  $[0, 1]$  to  $\mathbb{R}$  using an instance-specific scaling factor. This reverse flow normalization operation is identical to the one used in IFE [13].

### 7.2 Network architecture

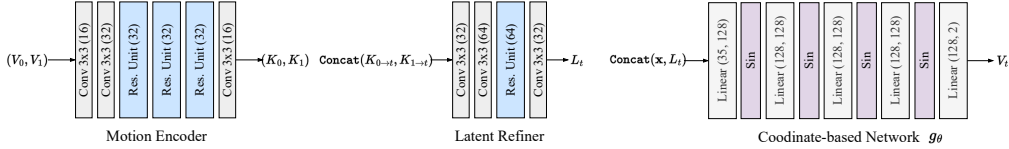


Figure 6: Details of the network architectures within the GIMM Module. The numbers in parentheses denote the output channel count for convolutional layers or the dimensionality shift from input to output for linear layers.

**GIMM module.** The architectural details of the networks used in GIMM are shown in Fig. 6. The Motion Encoder and Latent Refiner utilize a similar convolutional network architecture with residual units. Each Residual Unit consists of two convolutional layers with a skip connection. The major differences between them are the number of channels and residual units. On the other hand, the coordinate-based network  $g_\theta$  is designed as a five-layer SIREN [45], incorporating the motion latent  $L_t$  as an auxiliary input.

**Frame synthesis module.** Adapted from AMT-G [28], the framework of the Frame synthesis module is illustrated in Fig. 7. This module integrates two unique decoding stages: an adapted initial decoder and a revised final decoder, while the rest of the module’s architecture remains unchanged from AMT-G. The architectural specifics of these modified decoders are shown in Fig. 8.

### 7.3 Implementation details

In addition to experiments in the main text, we present more detailed implementations of GIMM and GIMM-VFI in this section.

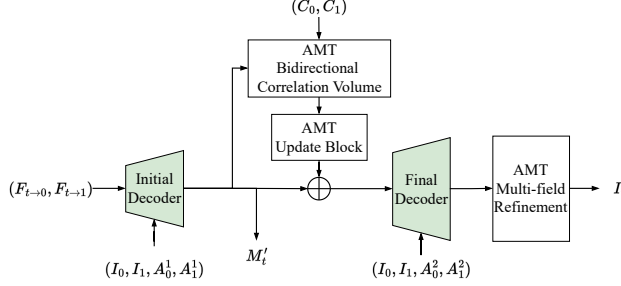


Figure 7: Overview of the frame synthesis module. The frame synthesis module conducts multi-scale flow refinements and predicts warping masks for interpolation, including the intermediate warping mask  $M'_t$  predicted by the initial decoder. It integrates the images and their pyramid features  $A_0^l, A_1^l | l \in 1, 2$  during decoding, updating predictions with correlation information from the Bidirectional Correlation Volume, which is constructed with correlation features  $(C_0, C_1)$ . Ultimately, we use the outputs from the Final Decoder to perform the final interpolation of  $I_t$  through the Multi-field Refinement block. This block is adapted from AMT-G [28]. Modified components are highlighted in green for clarity.

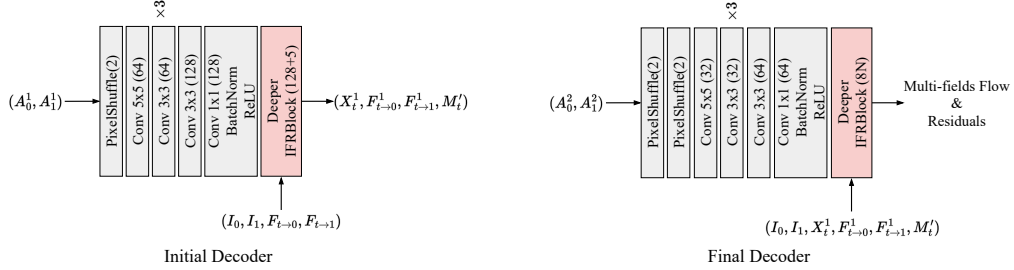


Figure 8: The network architectures of the modified decoders within the frame synthesis module. Unless specifically noted, each convolutional layer is activated by a PReLU function. The Deeper IFRBlock (highlighted in red) is based on the decoder architecture (IFRBlock) introduced in IFR-Net [25]. In particular, we enhance the original IFRBlock by adding two additional residual blocks to create the Deeper IFRBlock.

**GIMM training.** We begin by extracting optical flows from the training split of the Vimeo90K triplets dataset [51] using Flowformer [18]. With these extracted flows, we train GIMM, randomly cropping the flows to a resolution of  $256 \times 256$ . For each batch during training, we randomly select a timestep  $t$  from the set  $\{0, 0.5, 1\}$  to supervise. We set the batch size to 64, and train the model for 240 epochs with a learning rate of  $1 \times 10^{-4}$ , using 2 NVIDIA V100 GPUs.

**GIMM-VFI training.** We integrate the pre-trained GIMM module and flow estimator into the GIMM-VFI model for end-to-end training on the arbitrary-timestep interpolation task. We implement two variants of GIMM-VFI, using two different flow estimators: the RAFT [47] and FlowFormer [18], designated as GIMM-VFI-R and GIMM-VFI-F, respectively. However, both versions of GIMM-VFI share the same training process. Similar to previous works [52, 19], we train our model on the complete Vimeo90K septuplet split [51] for 60 epochs with a batch size of 32 and a learning rate of  $8 \times 10^{-5}$ . We randomly select triple subsets for training from each septuplet, following the same sampling strategy as previous research [52, 19]. We resize and randomly crop each frame into a resolution of  $224 \times 224$  and perform a series of augmentations including rotation, flipping, temporal order reversing and channel order reversing. We train our model on 8 NVIDIA V100 GPUs.

## 7.4 Training hyperparameters

In addition to the implementation details in Sec. 7.3, we summarize the training settings for both GIMM and GIMM-VFI in Tab. 4.

Table 4: **Training settings** for GIMM and GIMM-VFI.

Configuration	GIMM	GIMM-VFI
Optimizer		AdamW
Peak learning rate	1e-4	8e-5
Minimum learning rate	1e-4	8e-6
Epochs	240	60
Batch size per GPU	16	4
Weight decay	0	4e-5
Optimizer momentum	$\beta_1, \beta_2 = 0.9, 0.999$	
Learning rate schedule	$\times$	Cosine annealing
Warmup epochs	0	1
Training Resolution	$256 \times 256$	$224 \times 224$
Num. V100 GPUs	2	8

### 7.5 Qualitative results of GIMM motion modeling

We present additional qualitative results of GIMM motion modeling in Figure 9. The visualization showcases the modeled motion of GIMM and variants in the ablation study. Our observation confirms the effectiveness of GIMM’s design and is consistent with the results from the ablation study in the main text. For example, the head motion in Figure 9 significantly deteriorates with noises across all timesteps when forward warping is replaced or latent refinement is skipped.

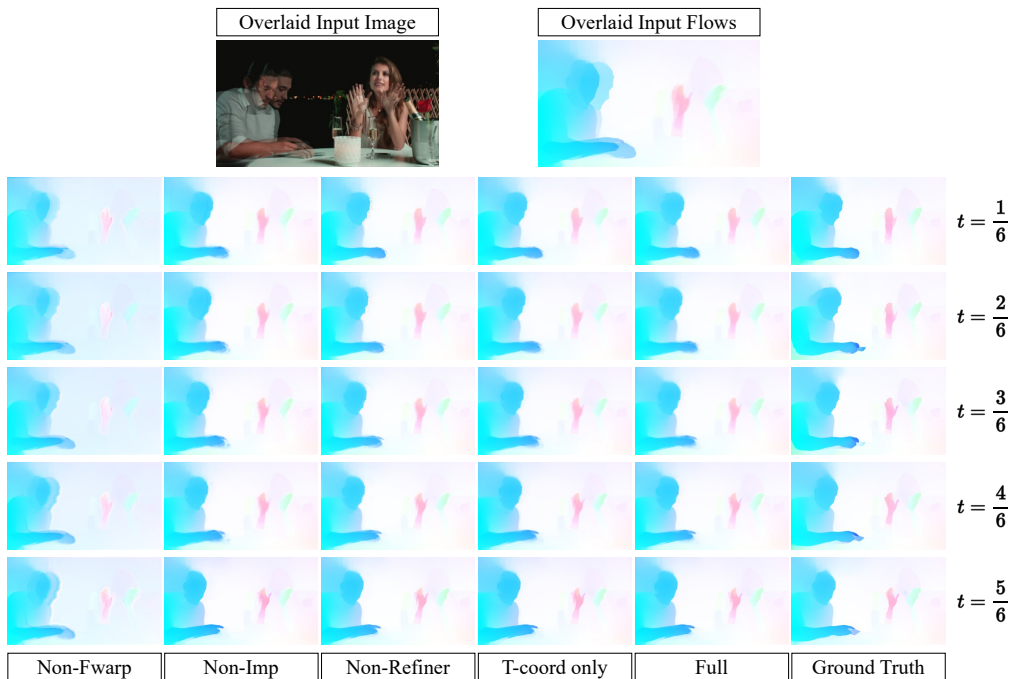


Figure 9: Visual comparisons for 6X motion modeling on the Vimeo-septuplet-flow. We compare GIMM with its model variants mentioned in the ablation study of the main text.

### 7.6 Broader impacts

We anticipate that our work will have several societal impacts. Firstly, our proposed method excels in continuous frame interpolation, which can be utilized in various real-world applications, such as creating special effects in movies and generating slow-motion videos. Secondly, our research may inspire further studies in video technology. This paper introduces a new method, GIMM-VFI, which employs the GIMM module for continuous motion modeling in video frame interpolation. GIMM could be adapted for other tasks like video compression and prediction. However, like other frame

interpolation methods, our approach has failure cases that could potentially result in the pollution of visual data on the internet.